Vibrational Spectroscopy 96 (2018) 46–51

Contents lists available at ScienceDirect

Vibrational Spectroscopy

journal homepage: www.elsevier.com/locate/vibspec

Photonic, spectroscopic properties and electronic structure of PTCDI-C8 organic nanostructure

Bayram Gündüz[a], Mustafa Kurban[b,*]

[a] Department of Science Education, Faculty of Education, Muş Alparslan University, 49250 Muş, Turkey
[b] Department of Electronics and Automation, Ahi Evran University, 40100 Kırşehir, Turkey

ARTICLE INFO

Article history:
Received 29 December 2017
Received in revised form 20 February 2018
Accepted 21 February 2018
Available online 27 February 2018

Keywords:
Optical techniques
Structure analysis
Photonic properties
Electronic properties
Density-functional theory

ABSTRACT

The changes in the structural, electronic, vibrational and photonic properties of *N*,*N*′-Dioctyl-3,4,9,10-perylenedicarboximide (PTCDI-C8) one-dimensional nanostucture have been investigated using experimental and theoretical techniques. The semi-empirical relations have been proposed for the calculation of the refractive index (n)from its measured and calculated energy gap (E_g) data. FT-IR and FT-Raman spectra characteristics and structural, spectroscopic and electronic properties such as HOMO-LUMO energies, harmonic frequencies, Mullkien atomic charges, dipole moments, radial distribution functions (RDFs) and coordination number of binary interactions were recorded with the aid of density functional theory (DFT) based on optimized structure for gas phase and different solvent environments. Moreover, ultraviolet-visible (UV–vis) spectral analysis and energy gaps has been carried out using experimental techniques and time-dependent (TD) DFT calculations. The results herein obtained reveal that PTCDI-C8 material is suitable for sensitivity applications due to its appropriate optoelectronic paramaters.

1. Introduction

Recently, organic semiconductors have widely used in many electronic, optoelectronic, and photonic applications [1] such as solar cells [2–5] photovoltaics [4,5] light emitting diodes [4,6] sensors [7,8], chemical sensors [9], vapour sensors [10], gas sensors [11,12] and photodetectors [13]. Among organic semiconductors, the perylenediimides (PTCDIs) have attracted great interest in the fabrication of optoelectronic devices such as transistors, light-emitting diodes and photovoltaic cells [14] becuse of their high thermal and photo-stability properties under visible light beam [15–22].

In the literature, a series of available perylene and its derivatives (PTCDI-M, where M = C5, C8, C10, BP2C10, OSC etc.) were studied in various electronic, photovoltaic and optoelectronic devices. Among these derivatives, *N*,*N*′-Dioctyl-3,4,9,10-perylenedicarboximide (PTCDI-C8) is a very important material for organic field effect transistors [23] and solar cells [24,25] as its mobility is higher than that of fullerenes. In this regard, various studies have been conducted on PTCDI-C8 nanostructure. For example, the effect of the thickness on the structural and optical properties of PTCDI-C8 thin films have been investigated using thermal evaporation technique and observed the high degree of molecular packing depending on the optical and structural properties [26]. PTCDI-C8 nanoribbons have been synthesized to investigate nonlinear optical properties for potential applications [27]. The molecular structure of PTCDI-C8 on different substrates has also been reported [28]. In addition, PTCDI-C8 have been performed as an acceptor material for photovoltaic and thin film transistor applications due to its better absorption properties [23,25,29].

The solute-solvent interactions are crucial to understand molecular behaviour because the interactions give rise to the significant changes in the chemical and physical characteristics of the solute from gas phase to solvent phase [30]. In the recent years, thermally evaporated PTCDI-C8 thin films with four different solvents (methanol, acetone, chlorobenzene, chloroform) have been experimentally researched [31]. In the study, the methanol treated vertical nanostructure was found to give the best efficiency on the solar cell performance. Therefore, the contributions from different physical and optoelectronic properties based on different solvent environments have still to be discussed. In this regard, the aim of the present study is to evaluate photonic, spectroscopic properties and electronic structure of PTCDI-C8 nanostucture using experimental technique and density functional theory (DFT)

* Corresponding author.
E-mail addresses: mkurbanphys@gmail.com, mkurban@ahievran.edu.tr (M. Kurban).

https://doi.org/10.1016/j.vibspec.2018.02.008
0924-2031/

approach. These properties were controlled with different solvents (ethanol, methanol, and chloroform). Firstly, we have analysed the Fourier Transform Infrared (FT-IR) and Fourier Transform Raman (FT-Raman) spectra characteristics, radial distribution functions (RDFs) and probability distributions in terms of coordination number of the binary interactions, the highest occupied molecular orbital (HOMO), the lowest unoccupied molecular orbital (LUMO) and the frontier molecular orbital energy gap (HOMO–LUMO difference in energy gap, E_g), Mullkien atomic charges of the small molecule using DFT calculations. The measured and calculated $E_g$values have been performed for different solvents. Using time-dependent (TD)-DFT method, the theoretically predicted the ultraviolet-visible (UV–vis), HOMO, LUMO and E_g of the nano-structure have been compared with the measured results. Different relations were also performed to calculate the optical refractive index (n) values and compared with measured values for different solvents. Later, the effects of the solvents on the mass extinction coefficient, $(\alpha h\vartheta)^2$curves based on photon energy (E), single oscillator energy (E_0), dispersion energy (E_d), constrat based on E, surface and volume energy loss functions (SELF and VELF) depend on the dielectric constant were experimentally investigated. Finally, we discussed these parameters based on different solvents for optoelectronic applications in detail.

2. Experimental details

2.1. The solutions of the PTCDI-C8 for various solvents

We purchased the PTCDI-C8 nanostructure material, which its fullname is *N*,*N*′-Dioctyl-3,4,9,10-perylenedicaroboximide, and solvents (ethanol, methanol and chloroform) from Sigma-Aldrich Co. We arranged the solutions of PTCDI-C8 nanostructure dissolved homogeneously in 8 mL volume of ethanol, methanol and chloroform solvents at 2.75 mM.

2.2. The UV-vis measurements

Then, we taken the UV–vis measurements of PTCDI-C8 solutions for different solvents using a Shimadzu Spectrophotometer (UV-1800, Japan) at room temperature.

2.3. Theoretical considerations

In here, we will give theoretical considerations for significant optical properties such as molar absorptivity (molar extinction coefficient), mass molar absorptivity (mass extinction coefficient), optical band gap, refractive index,

Molar absorptivity or molar extinction coefficient (ε) is an important optical parameter and plays role on UV–vis spectra of materials. The ε can be determined by Beer–Lambert law [32],

$$\varepsilon = \frac{\mathrm{Abs}}{\mathrm{cL}} \tag{1}$$

where Abs is absorbance, c is molar concentration and L is length of the optical path.

Mass is an efficient factor on molar absorptivity. Mass absorptivity or mass extinction coefficient (α_{mass}) gives molar extinction coefficient per unit molecular weight. The α_{mass} parameter is given by [33],

$$\alpha_{\mathrm{mass}} = \frac{\varepsilon}{\mathrm{M_A}} \tag{2}$$

where is M_A is the molecular weight.

Tauc model [34] estimates the optical transitions and optical band gap of materials. The optical band gap (E_g) is the most essential parameter of the optical parameters. The E_g of materials can be determined by Tauc model,

$$\alpha(\mathrm{E}) = \mathrm{A}(\mathrm{E} - \mathrm{E_g})^{\mathrm{n}} \tag{3}$$

where α is the absorption coefficient, E is photon energy, A is a constant. n determines the type of the optical transitions.

Refractive index (n) parameter is the most another esseintial parameter of the optical parameters and can be calculated based on reflectance (R) from the following equation,

$$\mathrm{n} = \sqrt{\frac{4\mathrm{R}}{(\mathrm{R}-1)^2} - \mathrm{k}^2} - \frac{\mathrm{R}+1}{\mathrm{R}-1} \tag{4}$$

where k depends on absorption coefficient and $k = \alpha\lambda/4\pi$.

There are two regions for refractive index dispersion including normal and abnormal dispersion region. The refractive index dispersion is analyzed with a multi oscillator model in abnormal region, while the refractive index dispersion is analyzed with a single oscillator model in normal region. The n dispersion is evaluated by the Wemple–DiDomenico equation [35,36],

$$\mathrm{n}^2 - 1 = \frac{\mathrm{E_0 E_d}}{\mathrm{E_0^2} - \mathrm{E}^2} \tag{5}$$

where E_0 is single oscillator energy (or average excitation energy) and E_d is dispersion energy.

M_{-1} and M_{-3} moments can be explained depending on single oscillator and dispersion energy and is given by [37],

$$\mathrm{M_{-1}} = \mathrm{M_{-3}} \mathrm{E_0^2} \tag{6}$$

and

$$\mathrm{M_{-3}} = \frac{\mathrm{M_{-1}^3}}{\mathrm{E_d^2}} \tag{7}$$

The optical oscillator strength (f) is another important parameter for optical transitions and is given by [36],

$$f = \mathrm{E_0 E_d} \tag{8}$$

The contrast (α_c) depends on normalised refractive index and shows the sensitivity of a material or device. The α_c is given by

$$\alpha_{\mathrm{c}} = 1 - \left(\frac{\mathrm{n_1}}{\mathrm{n_2}}\right)^2 \tag{9}$$

The surface and volume energy loss functions (SELF and VELF) depend on the dielectric constant are significant parameters. The SELF and VELF parameters can be determined with following equations [38],

$$SELF = \frac{\varepsilon_2^2}{(\varepsilon_1 + 1)^2 + \varepsilon_2^2} \tag{10}$$

and

$$VELF = \frac{\varepsilon_2^2}{\varepsilon_1^2 - \varepsilon_2^2} \tag{11}$$

where $\varepsilon_1 = n^2 - k^2$ and $\varepsilon_2 = 2nk$ are the real and imaginary parts of the dielectric constant, respectively.

3. Computational details

The structural, electronic and spectroscopic properties of the PTCDI-C8 have been investigated using DFT [39] at the B3LYP level [40–42]. The 6-311G (d, p) basis set has been used in the calculations. In order to test the validity and reliability of our calculations, CAM-B3LYP [43] functional were also tested for accuracy and efficiency of the calculations because B3LYP actually

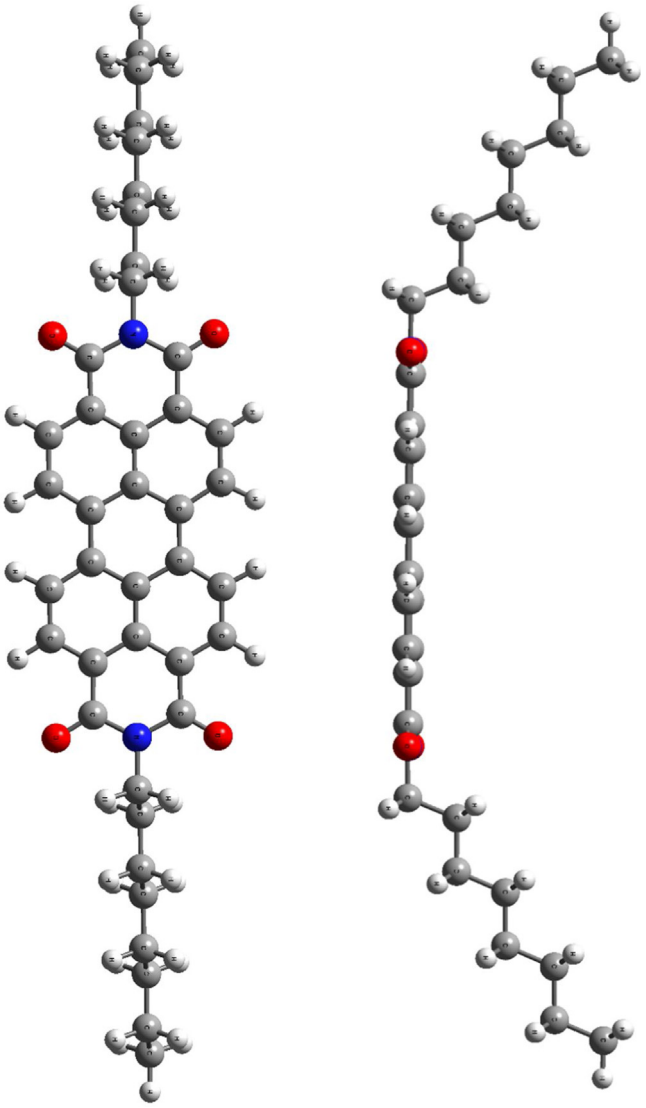

Fig. 1. Different views of optimized ground state geometry of PTCDI-C8 nanostructure calculated by B3LYP/6-311-G(d, p).

underestimates HOMO-LUMO gaps and underestimate excited-state energies [44–46]. The calculations have been performed using the GAUSSIAN09 program package [47]. Various spin multiplicities were investigated and it has been found that PTCDI-C8 have spin singlet as the most stable (minimum total energy). The structure is taken as the local minima on potential energy surface having positive vibration frequencies. After geometric optimization, TD-DFT method used to get maximum wavelengths and compared with the experimental UV, FT-IR absorption, HOMO, LUMO and E_g of the PTCDI-C8.

4. Results and discussion

4.1. Structural analysis

Optimized ground state structure and process of geometry optimization of the PTCDI-C8 with calculated by B3LYP/6-311-G (d, p) is shown in Figs. 1 and S1 in Supporting information, respectively. The positive vibrational spectra, that is no any kind of imaginary frequency, are found that the optimized geometry is located at stationary point on the potential energy surface. Calculated first three vibrational harmonic frequencies for gas phase are found to be 11.06, 11.48 and 15.23 cm^{-1}, respectively. The geometrical optimization results reveals that the structure with minimum total energy is the C_1 form. All the 258 fundamental modes of vibrations were found to be IR and Raman active suggesting that the molecule possesses a non-centro symmetric structure. For visual comparison the simulated FT-IR and FT-Raman spectra are shown in Figs. 2 and 3, respectively. As seen in Fig. 2, The IR spectra of the PTCDI-C8 exhibit the peaks at 1360 cm^{-1} (N—O symmetrics strech and C-H bending vibration), at 1616 cm^{-1} (ν(C=C, aromatic)), at 1688 cm^{-1} (C=O groups), at 1728 cm^{-1} (C=O stretch and carboxylic carbonyl groups), at 3008 cm^{-1} (aromatic C—H stretching and CH=CH double bonds) and at 3048 cm^{-1} (=C—H stretching). On the other hand, as seen in Fig. 3, the Raman spectra of the PTCDI-C8 exhibit the peaks at 1104 cm^{-1} (symmetrical and asymmetrical C—O streching ester vibrations), at 1328 cm^{-1} ($\delta(CH_3)$), at 1408 cm^{-1} (CH bending), at 1608 cm^{-1} (ring quadrant streching), at 1736 cm^{-1} (C=O stretching) and at 3008 cm^{-1} (CH_3 stretching). Obtained results suggest that the IR and Raman spectra of the PTCDI-C8 are almost the same for all solvents.

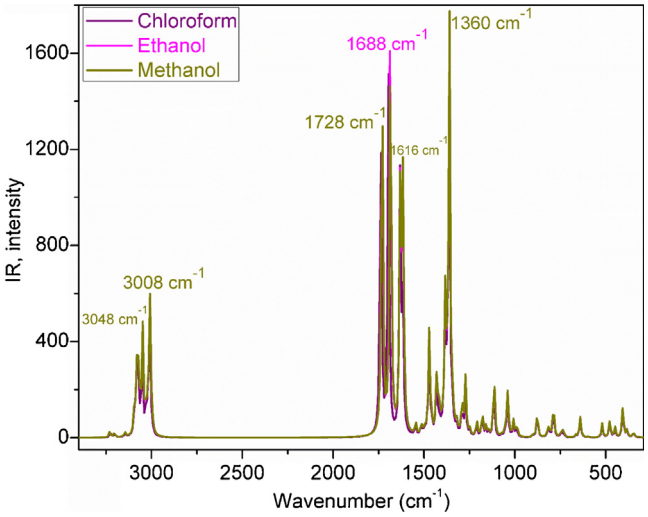

Fig. 2. FT-IR spectra of PTCDI-C8 nanostructure.

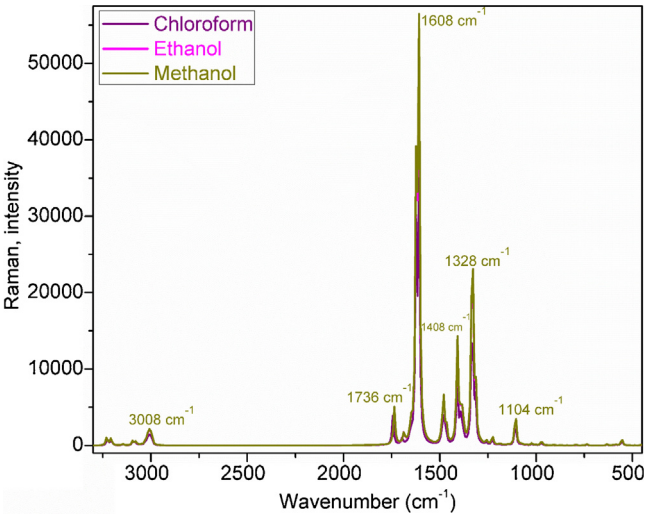

Fig. 3. FT-Raman spectra of PTCDI-C8 nanostructure.

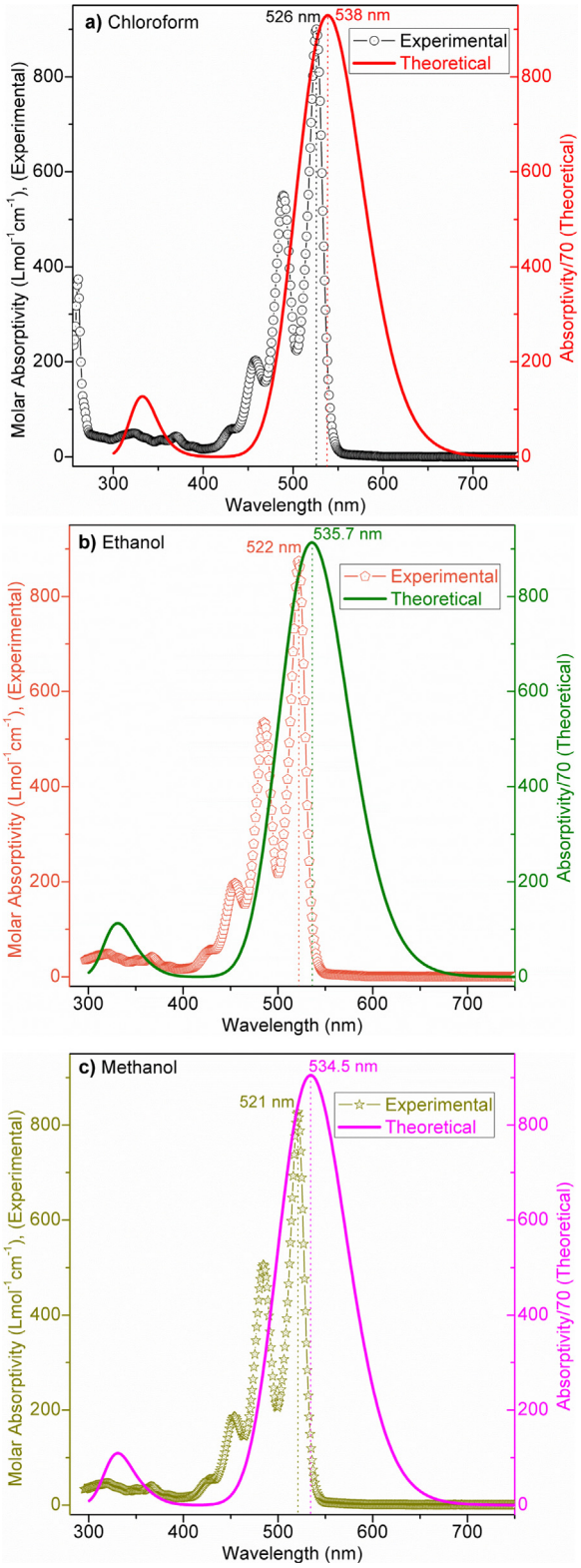

Fig. 4. The experimental and theoretical absorptivity spectra of PTCDI-C8 nanostructure for a) chloroform, b) ethanol and c) methanol solvents.

4.2. The absorbance and optical characteristics for various solvents

We explained the molar absorptivity or molar extinction coefficient in theoretical considerations section. We calculated absorptivity values of the PTCDI-C8 nanostructure for different solvents. The experimental and theoretical absorptivity spectra of the PTCDI-C8 for chloroform, ethanol and methanol solvents are shown in Fig. 4(a–c), respectively. As seen in Fig. 4(a–c), the measured absorptivity spectra of PTCDI-C8 solution dissolved in chloroform, ethanol and toluene solvents exhibit the maximum peak at 526, 522 and 521 nm, respectively. Obtained results suggest that the experimental and theoretical maximum peaks of the PTCDI-C8 solution are observed in visible region. The absorptivity spectra obtained from experimental studies are consistent with the absorptivity spectra obtained from theoretical studies (see Fig. 4). In addition, we performed one single benchmark for the excited state energies using CAM-B3LYP which is a range-separated functional. The maximum peak of absorptivity spectra is found to be 529.73 and 538.07 nm for CAM-B3LYP and B3LYP functionals, respectively. The mass absorptivity or mass extinction coefficient was explained in theoretical considerations section. The α_{mass} values of the PTCDI-C8 for chloroform, ethanol and methanol solvents were calculated from Eq. (2). Fig. S2 in Supporting information indicates the α_{mass} curves vs. photon energy $(E)$of the PTCDI-C8 for these solvents. As seen in Fig. S2, PTCDI-C8 for chloroform, ethanol and methanol exhibits the maximum α_{mass} peaks at 2.357, 2.376 and 2.380 eV, respectively.

The type of the optical transitions and optical band gaps of the PTCDI-C8 for chloroform, ethanol and methanol solvents were estimated by using Eq. (3). PTCDI-C8 nanostructure shows the allowed direct optical band gap. The allowed direct optical band gap gives more effective results than the indirect optical band gap for different solvents. For this, we plotted the $(\alpha h\vartheta)^2$ curves vs. E as seen in Fig. S3 in Supporting information and obtained its direct optical band gaps for different solvents. The direct optical band gaps of the PTCDI-C8 for chloroform, ethanol and methanol were found to be 2.275, 2.292 and 2.297 eV, respectively. This measured values are found to be compatible with calculated values (see Table 2). The PTCDI-C8 gives the lowest optical band gap with chloroform solvent, while the PTCDI-C8 gives the highest optical band gap with methanol solvent. These results suggest that the PTCDI-C8 is a good semiconductor material.

4.3. The refractive index and single oscillator model parameters for various solvents

We explained the refractive index (n) and single oscillator model in theoretical considerations section. The n values of the PTCDI-C8 for chloroform, ethanol and methanol solvents were obtained from Eq. (4). Fig. S4 in Supporting information shows the n curves vs. wavelength (λ). As seen in Fig. S4, the n values of the PTCDI-C8 for these solvents decrease with increasing wavelength. This behavior indicates that the PTCDI-C8 exhibits a normal dispersion region in the related regions. For this, we analyzed the refractive index dispersion of the PTCDI-C8 with a single oscillator model using Wemple-DiDomenico equation, which is the Eq. (5). We plotted the $(n^2\text{-}1)^{-1}$ vs. E^2 of the PTCDI-C8 to calculate the experimental verification of Eq. (5) (Supporting information, Fig. S5). The single oscillator energy (E_0) and the dispersion energy (E_d)values of the PTCDI-C8 were obtained from straight lines of Fig. S5 and given in Table 1. As seen in Table, the E_0values of the PTCDI-C8 for same solvents are 3.162, 3.206 and 2.747 eV, while the $E_d$values of the PTCDI-C8 for chloroform, ethanol and methanol are 7.906, 7.799 and 6.321 eV, respectively. These results indicate that the lowest E_0 and E_d values were obtained with methanol, while the highest E_0 and E_d values were obtained with ethanol.

The M_{-1} and M_{-3} moments of the PTCDI-C8 were calculated using Eqs. (6) and (7). Obtained the M_{-1} and M_{-3} moments are given in Table 1. As seen in Table 1, the lowest M_{-1} moment (2.302) is

Table 1
The single oscillator model of PTCDI-C8 nanostructure for chloroform, ethanol and methanol solvents.

Solvents	E_d (eV)	E_0 (eV)	M_{-1}	M_{-3} (eV^{-2})	f (eV^2)
Chloroform	7.906	3.162	2.500	0.250	25.00
Ethanol	7.799	3.206	2.433	0.237	25.00
Methanol	6.321	2.747	2.302	0.305	17.36

Table 2
The experimental direct optical band gaps (E_{gd}, eV)depending on different solvents and concentrations (mM) and the energy gaps (E_g, eV) for different solvents obtained from DFT and TD-DFT calculations.

Solvents	E_{gd}	DFT	TD-DFT	Molarities	[a]E_{gd}
Chloroform	2.275	2.510	2.521	**4.648**	2.206
Ethanol	2.292	2.503	2.518	**5.422**	2.190
Methanol	2.297	2.502	2.517	**6.507**	2.126

[a] Ref. [49].

observed for methanol, while the highest M_{-1} moment (2.500) is observed for chloroform. On the other hand, the lowest M_{-3} moment (0.237 eV^{-2}) is observed for ethanol, while the highest M_{-3} moment (0.305 eV^{-2}) is observed for methanol.

The optical oscillator strength values (f) of the PTCDI-C8 for different solvents were calculated from Eq. (8) and given in Table 1. As shown in Table 1, the f value (25 eV^2) of the PTCDI-C8 for both chloroform and ethanol solvents are the same, but the f value (17.361 eV^2) of the PTCDI-C8 for methanol is lower than that of the chloroform and ethanol solvents.

The refractive indexes of the PTCDI-C8 can also be calculated using optical band gaps with some relations [48] such as Moss, Hervé-Vandamme, Kumar-Singh, Ravindra and Reddy relations in addition to experimental method. The refractive indexes of the PTCDI-C8 for chloroform, ethanol and methanol solvents were calculated using these relations. We plotted these n values for different solvents (Supporting information, Fig. S6). The n values obtained for different solvents in the same relations are close to each other. But, the n values obtained from the related relations for the same solvents are different from each other. The n values obtained from Moss relation are the lowest, while the n values obtained from Reddy relation are the highest.

The contrast values of the PTCDI-C8 nanostructure for chloroform, ethanol and methanol were obtained from Eq. (9). Fig. S7 in Supporting information indicates the α_c plots vs. E. As seen in Fig. S7, the α_c varies with solvents and increases with increasing photon energy. The α_c values of the PTCDI-C8 for chloroform are the highest, while the α_c values of the PTCDI-C8 for methanol are the lowest. The PTCDI-C8 exhibits the sensitivity property and can be used in sensitivity applications.

The surface and volume energy loss functions of the PTCDI-C8 for chloroform, ethanol and methanol were determinde from the Eqs. (10) and (11), respectively. Fig. S8 in Supporting information shows the SELF and VELF curves vs. E. The SELF and VELF of the PTCDI-C8 exhibit the maximum peaks at 2.292, 2.314 and 2.318 eV, respectively. As seen in Fig. S8, the VELF values are close to the SELF values at lower photon energies, while the VELF values are higher than the SELF values at higher photon energies.

4.4. Electronic band structure

The energy gap which is HOMO-LUMO difference in energy, is an significant parameter in measuring the electron conductivity. The experimental direct optical band gaps (E_{gd})depending on different solvents and concentrations (mM) [49] and the energy gaps (E_g), obtained from DFT and TD-DFT calculations are tabulated in Table 2. The measured $E_{gd}$for chloroform, ethanol and methanol solvents are about 2.275, 2.292 and 2.297 eV, respectively, which is consistent with the theoretical $E_g$obtained from DFT (see Table 2). From the results, one can conclude that chloroform solvent with the lowering of the band gaps can be preferred for optoelectronic applications or devices, which prefer lower band gaps because the electronic transfer in the molecule PTCDI-C8 is easier. It implies that the $E_g$for chloroform solvent compared to that of other solvent allows easy excitation of electrons from HOMO to LUMO. We also performed one single benchmark for the excited state energies using CAM-B3LYP which is a range-separated functional. The calculated HOMO-LUMO energy gap with CAM-B3LYP are found to change dramatically (approximately 2-fold) compared to B3LYP. In addition, E_g decreases with increasing the size of the materials at the nanoscale (see Table 2). This is the most remarkable feature of nano material because we have already observed the same properties in our previous theoretical calculations related to small clusters [50].

4.5. Mulliken atomic charges and dipole moments

The Mulliken atomic charges (MAC) have a significant for quantum mechanical applications. MAC of PTCDI-C8 compound were gathered in Table 3. The charges of the atoms in the different

Table 3
Mullkien atomic charges of PTCDI-C8 nanostructure.

Atoms	Mulliken atomic charges	Atoms	Mulliken atomic charges
O1	−0.345759	C45	−0.286058
O2	−0.346063	C46	−0.286016
O3	−0.346712	H47	0.095612
O4	−0.346213	H48	0.095626
N5	−0.499229	H49	0.095611
N6	−0.498829	H50	0.095641
C7	−0.030921	H51	0.111779
C8	−0.030936	H52	0.111670
C9	0.003887	H53	0.111546
C10	0.004334	H54	0.111602
C11	0.004839	H55	0.139429
C12	0.004753	H56	0.137600
C13	0.134556	H57	0.137491
C14	0.133874	H58	0.138346
C15	−0.278458	H59	0.118032
C16	−0.276832	H60	0.115078
C17	−0.276535	H61	0.118747
C18	−0.276345	H62	0.116085
C19	−0.039526	H63	0.107763
C20	−0.039523	H64	0.106964
C21	−0.040057	H65	0.106845
C22	−0.039845	H66	0.107166
C23	−0.004973	H67	0.100907
C24	−0.005029	H68	0.104019
C25	−0.004335	H69	0.100891
C26	−0.004592	H70	0.104123
C27	0.537011	H71	0.100954
C28	0.534678	H72	0.101833
C29	0.532726	H73	0.101731
C30	0.533921	H74	0.100824
C31	−0.080119	H75	0.102777
C32	−0.079495	H76	0.101614
C33	−0.197154	H77	0.102792
C34	−0.197610	H78	0.101599
C35	−0.215527	H79	0.104930
C36	−0.215769	H80	0.103928
C37	−0.207392	H81	0.104882
C38	−0.207385	H82	0.103885
C39	−0.199797	H83	0.103536
C40	−0.199763	H84	0.100612
C41	−0.201985	H85	0.100838
C42	−0.201952	H86	0.103485
C43	−0.224024	H87	0.100568
C44	−0.223995	H88	0.100816

positions show different charge with each other for some carbon atoms. For example, MAC of Carbon atom is mostly negative in PTCDI-C8 compound, however, the value of the average MAC of this atom is positive in PTCDI-C8 compound when carbon atom combined with O and N atoms. The C27 atom exhibits a positive charge the value of MAC is bigger than others. Hydrogen atom exhibits a positive charge because it is an acceptor atom.

The dipole moments are other important electronic properties. The bigger the dipole moment represents the stronger intermolecular interaction. The highest value of component of dipole moment along the z-axis (μ_z = 0.1436 Debye) predicts large charge separation in PTCDI-C8 compound. The corresponding total dipole moment has been calculated to be 0.1503 Debye.

4.6. Radial distribution function and probability density

Fig. S9 in Supporting information shows the radial distribution functions (RDFs) analysis for the carbon–carbon (C—C), carbon–hydrogen (C—H), carbon–oxygen (C—O), carbon–nitrogen (C—N) hydrogen–hydrogen (H—H) interactions of PTCDI-C8 in chloroform solvent. The RDFs is calculated for each atomic pairs of optimized PTCDI-C8 molecule. One can see that C—H has a narrower and higher distribution than the other pair interactions because of the weaker bond and the low atomic weight of the H atom. For C atoms, C—C is shorter than C—H, C—O and C—N interactions; for H, H—H is shorter than C—H. For all of the combinations, C—H has stronger interactions than the other ones. To study the influence of interactions of the atoms in the molecule, we also performed the probability distribution depending on the coordination number (Supporting information, Fig. S10). The coordination number of C—N and C—O interactions significantly decrease; for C—C and C—H interactions we have observed some fluctuations.

5. Conclusions

PTCDI-C8 small organic molecule have been investigated using experimental and theoretical techniques. The results showed that the structure with minimum total energy is the C_1 form. The maximum peak of experimental molar extinction coefficients for different solvent enviroments is found to be compatible with theoretical value. The refractive index values increase depending on the variation of solvent environments from methanol to chloroform and decrease with increasing wavelength. Predicted energy gap values for solvent are also agreement with the experimental data. PTCDI-C8 nanostructure shows the allowed direct optical band gap. The charges of the atoms in the different positions show different charge with each other for some carbon atoms. In addition, C—H interactions has a narrower and higher distribution.

Acknowledgments

The numerical calculations reported in this paper were partially performed at TUBITAK ULAKBIM, High Performance and Grid Computing Centre (TRUBA resources). This work was supported by the Ahi Evran University Scientific Research Projects Coordination Unit. Project Number: TBY.C1.17.001 and the Management Unit of Scientific Research Projects of Muş Alparslan University (MUSBAP) under Project 0001, Turkey.

Appendix A. Supplementary data

Supplementary material related to this article can be found, in the online version, at doi:https://doi.org/10.1016/j.vibspec.2018.02.008.

References

[1] C. Xie, P. You, Z. Liu, L. Li, F. Yan, Light Sci. Appl. 6 (2017) e1702.
[2] T. Hori, T. Masuda, N. Fukuoka, T. Hayashi, Y. Miyake, T. Kamikado, H. Yoshida, A. Fujii, Y. Shimizu, M. Ozaki, Org. Electron. 13 (2012) 335.
[3] S. Rajaram, R. Shivanna, S.K. Kandappa, K.S. Narayan, J. Phys. Chem. Lett. 3 (2012) 2405.
[4] A.D. Sio, C. Lienau, Phys. Chem. Chem. Phys. 19 (2017) 18813.
[5] M.Y. Ameen, T. Abhijith, D. Susmita, S.K. Ray, V.S. Reddy, Org. Electron. 14 (2013) 554.
[6] M. Neghabia, A. Behjata, Curr. Appl. Phys. 12 (2012) 597.
[7] F. Aziz, M.H. Sayyad, K. Sulaiman, B.Y. Mailis, K.S. Karimov, Z. Ahmad, G. Sugandi, Meas. Sci. Technol. 23 (2012) 014001.
[8] M. Murugavelu, P.K.M. Imran, K.R. Sankaran, S. Nagarajan, Mater. Sci. Semicon. Proc. 16 (2013) 461.
[9] D. Liu, Y. Chu, X. Wu, J. Huang, Sci. China Mater. 60 (2017) 977.
[10] R.N. Gillanders, D.W. Ifor, G.A. Samuel, Turnbull, Sens. Actuators B: Chem. 245 (2017) 334.
[11] Y. Huang, R. Yuan, S. Zhou, J. Mater. Chem. 22 (2012) 883.
[12] Y. Huang, L. Fu, W. Zou, F. Zhang, New J. Chem. 36 (2012) 1080.
[13] J.B. Wang, W.L. Li, B. Chu, C.S. Lee, Z.S. Su, G. Zhang, S.H. Wu, F. Yan, Org. Electron. 12 (2011) 34.
[14] C. Kufazvinei, M. Ruether, J. Wang, W. Blau, Org. Electron. 10 (2009) 674.
[15] B. Gündüz, Opt. Mater. 36 (2013) 425.
[16] C.C. Chao, M.K. Leung, J. Org. Chem. 70 (2005) 4323.
[17] L. Fan, Y. Xu, H. Tian, Tetrahedron Lett. 46 (2005) 4443.
[18] H. Dinçalp, Ş. Kızılok, S. İçli, Dyes Pigm. 86 (2010) 32.
[19] R.T. Weitz, K. Amsharov, U. Zschieschang, E.B. Villas, D.K. Goswami, M. Burghard, H. Dosch, M. Jansen, K. Kern, H. Klauk, J. Am.Chem. Soc. 130 (2008) 4637.
[20] Z. Yuan, J. Li, Y. Xiao, Z. Li, X. Qian, J. Org. Chem. 75 (2010) 3007.
[21] G. Boobalan, P. Mohamed Imran, S. Nagarajan, Chin. Chem. Lett. 23 (2012) 149.
[22] C.W. Struijk, A.B. Sievel, J.E.J. Dakhorst, M.V. Dijk, P. Kimkes, R.B.M. Koehorst, H. Donker, T.J. Schaafsma, S.J. Picken, A.M.W. Craats, J.M. Warman, H. Zuilhof, E.J. Sudholter, J. Am. Chem. Soc. 122 (45) (2000) 11057.
[23] P.R.L. Malenfant, C.D. Dimitrakopoulos, J.D. Gelorme, L.L. Kosbar, T.O. Graham, A. Curioni, W. Andreoni, Appl. Phys. Lett. 80 (2002) 2517.
[24] A.K. Pandey, K.N.N. Unni, J.-M. Nunzi, Thin Solid Films 511 (2006) 529.
[25] S. Karak, S.K. Ray, A. Dhar, Solar Energy Mater. Solar Cells 94 (2010) 836.
[26] R. Rahimi, V. Narang, D. Korakakis, Int. J. Photoenergy 2013 (2013) 205105.
[27] T. Abhijith, M. Yoosuf Ameen, V.S. Reddy, IOP Conf. Ser.: Mater. Sci. Eng. 73 (2015) 012052.
[28] K. Lament, W. Kaminski, P. Mazur, S. Zuber, A. Ciszewski, Appl. Surf. Sci. 304 (2014) 50.
[29] S. Karak, V.S. Reddy, S.K. Ray, A. Dhar, Org. Electron. 10 (2009) 1006.
[30] Y. Liu, H.C. Du, G. Wang, et al., Int. J. Quantum Chem. 111 (2011) 1115.
[31] S. Pradhan, J. Redwine, J.T. McLeskey, J.A. Dhar, Thin Solid Films 562 (2014) 423.
[32] A. Beer, Ann. Phys. 86 (1852) 78.
[33] Y. Li, N. Scales, R.E. Blankenship, R.D. Willows, M. Chen, Biochim. Biophys. Acta 2012 (1817) 1292.
[34] J. Tauc, A. Menth, J. Non-Cryst. Solids 569 (1972) 8.
[35] S.H. Wemple, M. DiDomenico, Phys. Rev. B 3 (1971) 1338.
[36] S.H. Wemple, M. DiDomenico, Phys. Rev. Lett. 23 (1969) 1156.
[37] J. Aranda, J.L. Morenza, J. Esteve, J.M. Codina, Thin Solid Films 120 (1984) 23.
[38] G.L. Tan, L.K. DeNoyer, R.H. French, M.J. Guittet, M. Gautier-Soyer, Mater. Sci. Eng. 294–296 (2000) 867.
[39] W. Kohn, L.J. Sham, Phys. Rev. 140 (1965) A1133.
[40] A.D. Becke, Phys. Rev. A 38 (1988) 3098.
[41] S.H. Vosko, L. Vilk, M. Nusair, Can. J. Phys. 58 (1980) 1200.
[42] C. Lee, W. Yang, R.G. Parr, Phys. Rev. B 37 (1988) 785.
[43] T. Yanai, D.P. Tew, N.C. Handy, Chem. Phys. Lett. 393 (2004) 51.
[44] M.E. Foster, B.M. Wong, J. Chem. Theory Comput. 8 (2012) 2682.
[45] A.P. Basile, F.E. Curchod, Alberto Fabrizio, L. Floryan, C. Corminboeuf, J. Phys. Chem. Lett. 6 (1) (2015) 13.
[46] E. Tanış, E.B. Şaş, M. Kurban, M. Kurt, J. Mol. Struct. 1154 (2018) 301.
[47] M.J. Frisch, G.W. Trucks, H.B. Schlegel, G.E. Scuseria, M.A. Robb, J.R. Cheeseman, G. Scalmani, V. Barone, B. Mennucci, G.A. Petersson, et al., Gaussian 09, Revision B.01, Gaussian, Inc., Wallingford, CT, 2009.
[48] S.K. Tripathy, Opt. Mater. 46 (2015) 240.
[49] E. Erdoğan, B. Gündüz, Electron. Mater. Lett. 12 (2016) 773.
[50] M. Kurban, Ş. Erkoç, J. Comput. Theor. Nanosci. 12 (2015) 2605.